ACS OMEGA

http://pubs.acs.org/journal/acsodf

Article

Preparation of Multicolor Biomass Carbon Dots Based on Solvent Control and Their Application in Cr(VI) Detection and Advanced Anti-Counterfeiting

Shipeng Wang, Haoran Zhao, Jinliang Yang, Yahui Dong, Shaozheng Guo, Qian Cheng,* Yu Li,* and Shouxin Liu*

Cite This: *ACS Omega* 2023, 8, 6550−6558

Read Online

ACCESS | Metrics & More | Article Recommendations | Supporting Information

ABSTRACT: Multicolor fluorescent carbon dots (CDs) have received widespread attention due to their excellent fluorescence performance and promising prospects in anti-counterfeiting and sensing detection. To date, most of the multicolor CDs synthesized are derived from chemical reagents; however, the overuse of chemical reagents during the synthesis process will pollute the environment and limit their application. Herein, multicolor fluorescent biomass CDs (BCDs) were prepared by a one-pot ecofriendly solvothermal method, with spinach as the raw material based on solvent control. The as-obtained BCDs can emit blue, crimson, grayish white, and red luminescence, and their quantum yields (QYs) are 8.9, 12.3, 10.8, and 14.4%, respectively. The results of the characterization of BCDs reveal that the regulating mechanism for multicolor luminescence is mainly ascribed to the change of the boiling point and polarity of solvents, which changes the carbonization process of polysaccharides and chlorophyll in spinach, resulting in the altered particle size, surface functional groups, and porphyrin luminescence properties. Further research reveals that blue BCDs (BCD1) show an excellent sensitive and selective response to Cr(VI) in a concentration scale of 0−220 μM with a detection limit (LOD) of 0.242 μM. More importantly, the intraday and interday relative standard deviation (RSD) values were less than 2.99%. The recovery rate of the Cr(VI) sensor for tap water and river water is 101.52−107.51%, which indicates that the sensor has the advantages of high sensitivity, selectivity, rapidity, and reproducibility. Consequently, different multicolor patterns are obtained by using the obtained four BCDs as fluorescent inks, which exhibit beautiful landscape and advanced anti-counterfeiting effects. This study provides a low-cost and facile green synthesis strategy for multicolor luminescent BCDs and proves that BCDs have broad application prospects in ion detection and advanced anti-counterfeiting.

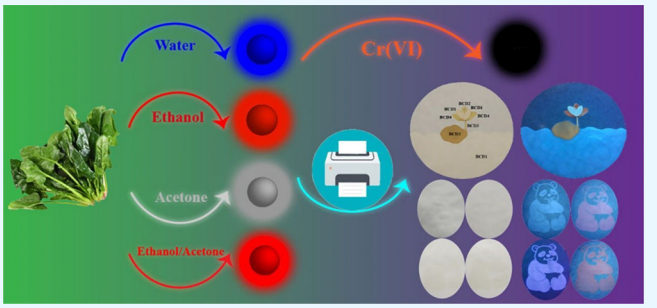

1. INTRODUCTION

CDs, as a new type of photoluminescent nanomaterials, have received widespread attention due to their excellent luminescence performance, low toxicity, high biocompatibility,[1,2] and potential application prospects in sensing,[3] biological imaging,[4] drug delivery,[5] photocatalysis,[6] and anti-counterfeiting.[7] Compared with the CDs from chemical reagents, BCDs have progressive advantages because of the simple synthesis method, ecofriendliness, and readily available raw materials, consistent with the idea of environmental protection and sustainable development. However, so far, the as-gained CDs from biomass materials mainly emit blue or green fluorescence,[8,9] which seriously hinders their development and application in bioimaging and anti-counterfeiting. Therefore, it is urgent to figure out a new strategy to prepare long-wavelength-emitting or multicolor luminous BCDs.

In nature, chlorophyll is rich in porphyrins and exhibits strong near-infrared absorption and emission. Unfortunately, chlorophyll cannot be directly used as a fluorescent material due to its hydrophobic and unstable nature. It has been documented that the degradation of chlorophyll occurs under light, acid, alkali, oxidant, and other conditions.[10,11] Interestingly, the fluorescence characteristics of porphyrins provide a new idea for the preparation of long-wavelength carbon dots. For example, Wang et al.[12] prepared single-excitation dual-emission red CDs with emission wavelengths of 487 and 676 nm by the solvothermal method, using holly leaf as the carbon source, and achieved the accurate detection of Hg^{2+} in living cells. In addition, Chinese cabbage[13] and Mulberry leaf[14] derived red-emissive carbon dots were studied and expected to

Received: October 27, 2022
Accepted: February 2, 2023
Published: February 10, 2023

https://doi.org/10.1021/acsomega.2c06942
ACS Omega 2023, 8, 6550−6558

Scheme 1. Illustration of the Preparation Process of Multicolor Fluorescent BCDs

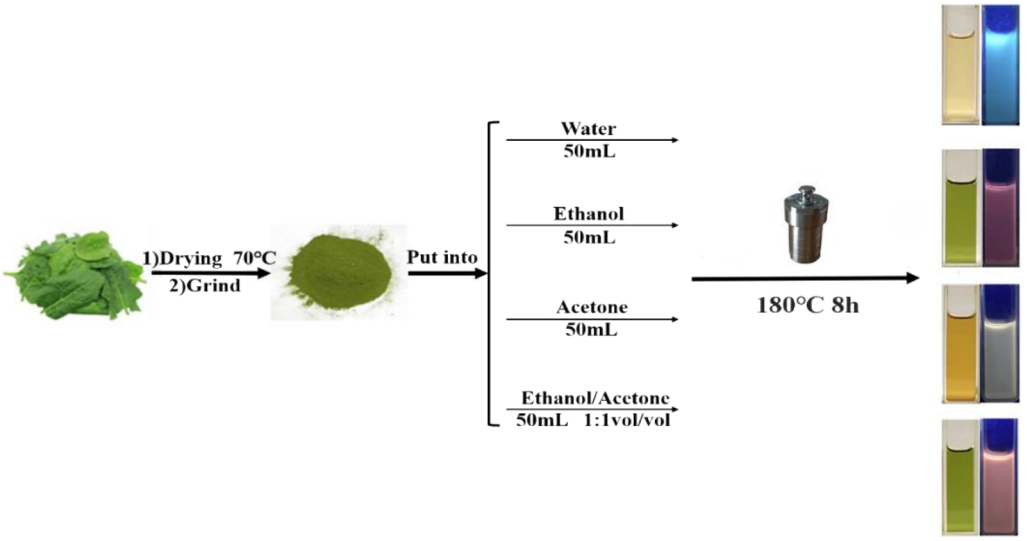

be used for fabric and fluorescent probes. The above research reveals that the preparation process of red CDs from leaves uses organic solvents such as ethanol, but the mechanism of red fluorescence has not been systematically investigated. Simultaneously, multicolor biomass CDs are rarely studied.

Herein, four BCDs with single excitation and double emission characteristics were synthesized by a one-pot solvothermal method using spinach as the carbon source based on the solvent control strategy. The maximum emission peak of the obtained multicolor BCDs changed from blue light to yellow-red light under 365 nm excitation, which almost covered the whole range of the visible spectrum. Moreover, according to the boiling point and polarity of the reaction solvents, the regulating mechanism for tunable luminescence was investigated. Consequently, the selectivity and sensitivity of BCD1 for metal ion detection were analyzed. In addition, four multicolor BCDs as fluorescent inks for anti-counterfeiting application were explored. This study proposed a facile and ecofriendly synthesis strategy for multicolor luminescent BCDs and proved that they have potential applications in sensing and anti-counterfeiting.

2. MATERIALS AND METHODS

2.1. Materials. Spinach was obtained from a local supermarket (Harbin, China) and served as the raw material. Ethanol, acetone, $CoCl_2$, $MgCl_2$, $MnCl_2$, $CuCl_2$, $FeCl_3$, $FeCl_2$, $CaCl_2$, $AgNO_3$, $K_2Cr_2O_7$, $Zn(NO_3)_2{\cdot}6H_2O$, $Cd(NO_3)_2{\cdot}4H_2O$, $Ni(NO_3)_2{\cdot}6H_2O$, $Ba(NO_3)$, $Pb(NO_3)_2$, $Al(NO_3)_3{\cdot}9H_2O$, $Cr(NO_3)_3{\cdot}9H_2O$, NaCl, NaBr, KCl, $NaClO_2$, $Na_2SiO_3{\cdot}9H_2O$, Na_2SO_3, and Na_2CO_3 were purchased from XinTian Chemical Reagents Ltd. (Harbin, China). Deionized water used here was self-made in our lab through a Kertone-mini water purification system (Clever-Q30 UT, Zhiang instrument (Shanghai) Co., Ltd) throughout the experiments. All reagents were of analytical grade and used directly without any further purification.

2.2. Preparation of Multicolor Fluorescent BCDs. Multicolor fluorescent BCDs were synthesized by a one-step solvothermal method using fresh spinach leaves as the carbon source based on reaction solvent control, and the preparation process is shown in Scheme 1. In detail, first, the fresh spinach leaves were cut into small pieces and dried at 70 °C. The dried pieces were ground into powders. Second, 0.2 g spinach leaf powders was dissolved in 50 mL of deionized water and ultrasonicated for 30 min. Subsequently, the mixture was transferred to a 100 mL Teflon-lined autoclave and heated at 180 °C for 8 h. After the reaction solution was naturally cooled to room temperature, the mixture was centrifuged at 8000 rpm for 10 min. Then, the supernatant was filtered by a sterile needle filter (aperture, 0.22 μm) to obtain a rough BCD1 (blue biomass carbon dots) solution. Third, the prepared rough BCD1 solution was then treated with a dialysis bag for 6 days to remove impurities. Finally, BCD1 powder was obtained by freeze-drying. BCD2 (crimson), BCD3 (grayish white), and BCD4 (red) were prepared by a synthesis process similar to that of BCD1, except that deionized water was changed into anhydrous ethanol, acetone, and the mixture of anhydrous ethanol and acetone (vol 1:1), respectively.

2.3. Characterization. TEM images were acquired using a Tecnai G2 F20 electron microscope (FEI, Holland) with an accelerating voltage of 200 kV. The XRD patterns of CDs were determined using a DMax/-RB2500V X-ray diffractometer (Rigaku Co., Japan) with Cu−Kα radiation (λ = 1.54056 Å). FT-IR spectra were obtained using a Perkin Elmer TV1900 instrument (Waltham, MA, USA). The fluorescence spectra were measured by an LS55 fluorescence spectrometer. Ultaviolet−visible (UV−vis) absorption spectroscopy was performed using a TU-1901 spectrophotometer (Beijing Purkinje General Instrument Co., Ltd., China). XPS of CDs was performed using K-Alpha with Al X-rays at 140 W (THERMO, USA).

2.4. Fluorescence Assays of Cr(VI). The sensitivity of Cr(VI) was explored in a phosphate buffer solution (0.1 M, pH = 8) at room temperature. In a typical process, 2 mL of BCD1 solution (10 μg/mL) was added to 1 mL of phosphate buffer solution, followed by various concentrations of Cr(VI) ions to obtain a dilute solution. The resultant homogeneous solution was incubated at room temperature for 15 min; the fluorescence intensity of the blank sample and different concentrations of Cr(VI) additive samples was measured under a UV lamp (400 nm), respectively. All the experiments were conducted at room temperature and repeated three times. The intraday and interday accuracy and repeatability of the sensor based on BCD1 for Cr(VI) were explored using three

https://doi.org/10.1021/acsomega.2c06942
ACS Omega 2023, 8, 6550−6558

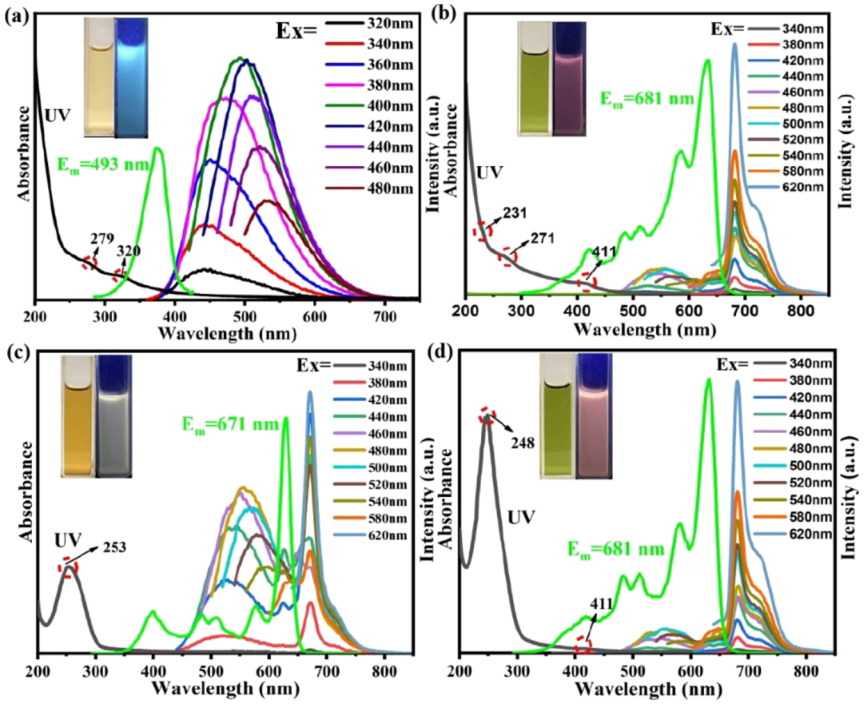

Figure 1. UV−visible absorption, fluorescence excitation, and emission spectra at different excitation wavelengths of BCDs. (a) BCD1, (b) BCD2, (c) BCD3, and (d) BCD4.

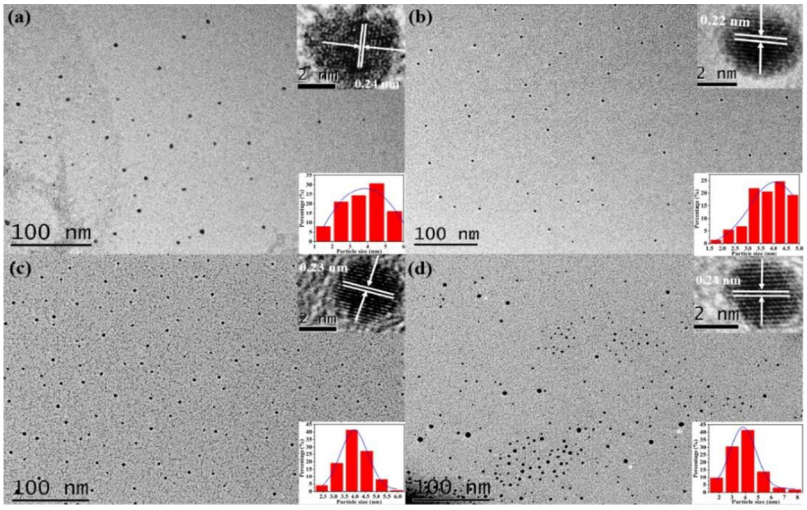

Figure 2. TEM images of BCDs. (a) BCD1, (b) BCD2, (c) BCD3, and (d) BCD4; the insets are the corresponding particle size distribution.

quality control samples, with the Cr(VI) concentration of low (20 μM), medium (40 μM), and high (60 μM), under optimal conditions, which were assessed within 1 day and on five consecutive days.

2.5. Environmental Water Samples with Quantitative Cr(VI) Detection. To evaluate the sensing capability of BCD1 in environmental water samples, river water and tap water were collected from the Majiagou River (Harbin, China) and our laboratory, respectively. Further, the luminescence intensities were measured at 400 nm excitation wavelength. The tap water samples were boiled for 5 min to remove the residual chlorine. Then, all the water samples were centrifuged at 10,000 rpm for 10 min and passed through a 0.22 μm membrane filter to eliminate the insoluble components. After that, different concentrations of Cr(VI) standard solutions were added into the above water samples to calculate the recovery rate of Cr(VI) in the real water samples. The relative standard deviation (RSD) was determined after five acquisition of data under similar experimental conditions.

3. RESULTS AND DISCUSSION

3.1. Fluorescence Properties of the BCDs. Four tunable luminescent BCDs were obtained using spinach as the carbon source based on reaction solvent control; the UV absorption spectra show that all the four samples have strong absorption peaks in the UV region of 240−280 nm, corresponding to the $\pi-\pi^*$ electronic transition of the C═C bond (shown in Figure.1). In addition, BCD1 has a weak absorption peak at 320 nm, corresponding to the $n-\pi^*$ electron transition of the C═O bond, which proves that carbon nuclei with a certain

https://doi.org/10.1021/acsomega.2c06942
ACS Omega 2023, 8, 6550−6558

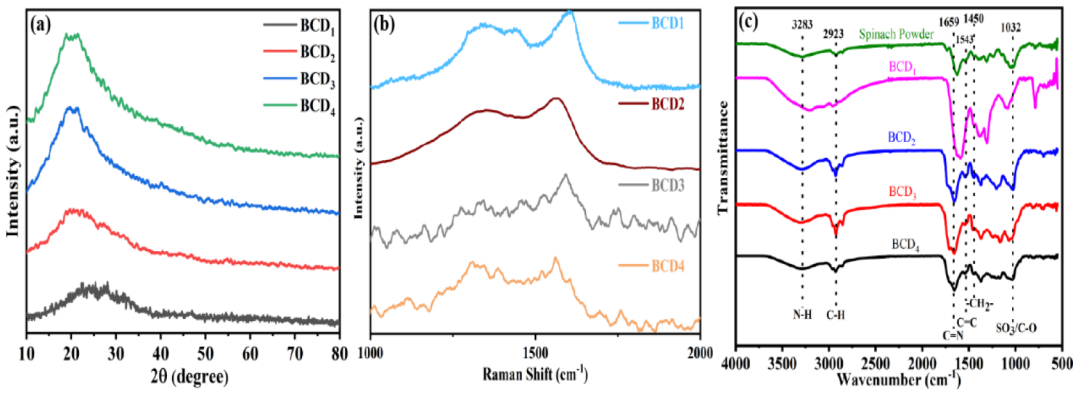

Figure 3. Spectra of BCDs: (a) XRD, (b) Raman, and (c) FTIR.

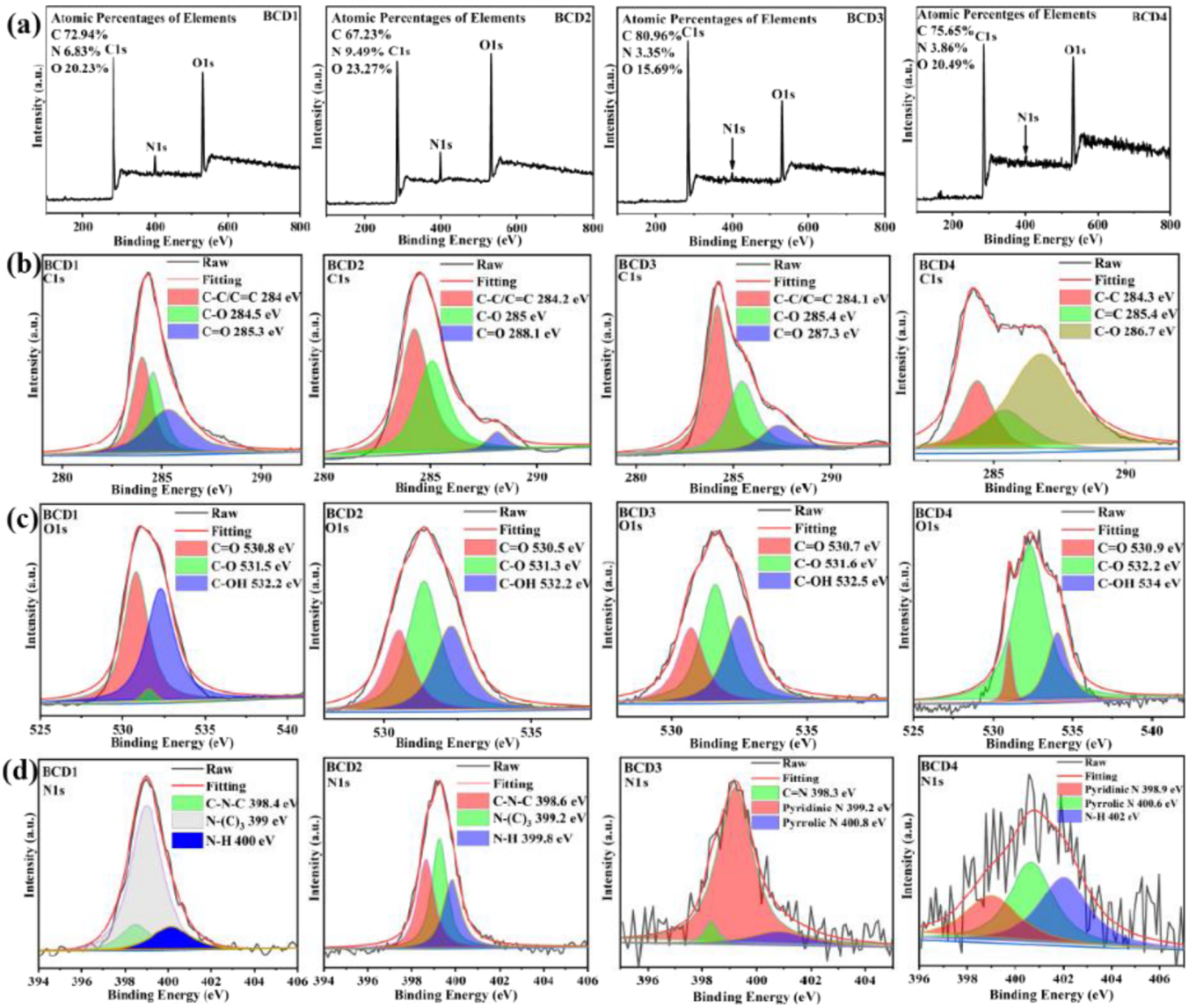

Figure 4. XPS analysis of BCD1, BCD2, BCD3, and BCD4. (a) Survey scan, (b) C 1s, (c) O 1s, and (d) N 1s.

conjugated structure are formed in the dehydration condensation reaction.[15,16] Both BCD2 and BCD4 present weak absorption peaks at 411 nm, which were attributed to the $n \rightarrow \pi^*$ electronic transition of the C═O bond in the chlorophyll-derived porphyrin structure.[17]

Four BCDs with different luminescence properties are found in the fluorescence emission spectra (shown in Figure 1). BCD1 shows a blue-to-yellow emission region (400−600 nm) with an excitation wavelength dependence and QY of 8.9% (Figure 1a); the maximum fluorescence peak is located at 493

https://doi.org/10.1021/acsomega.2c06942
ACS Omega 2023, 8, 6550−6558

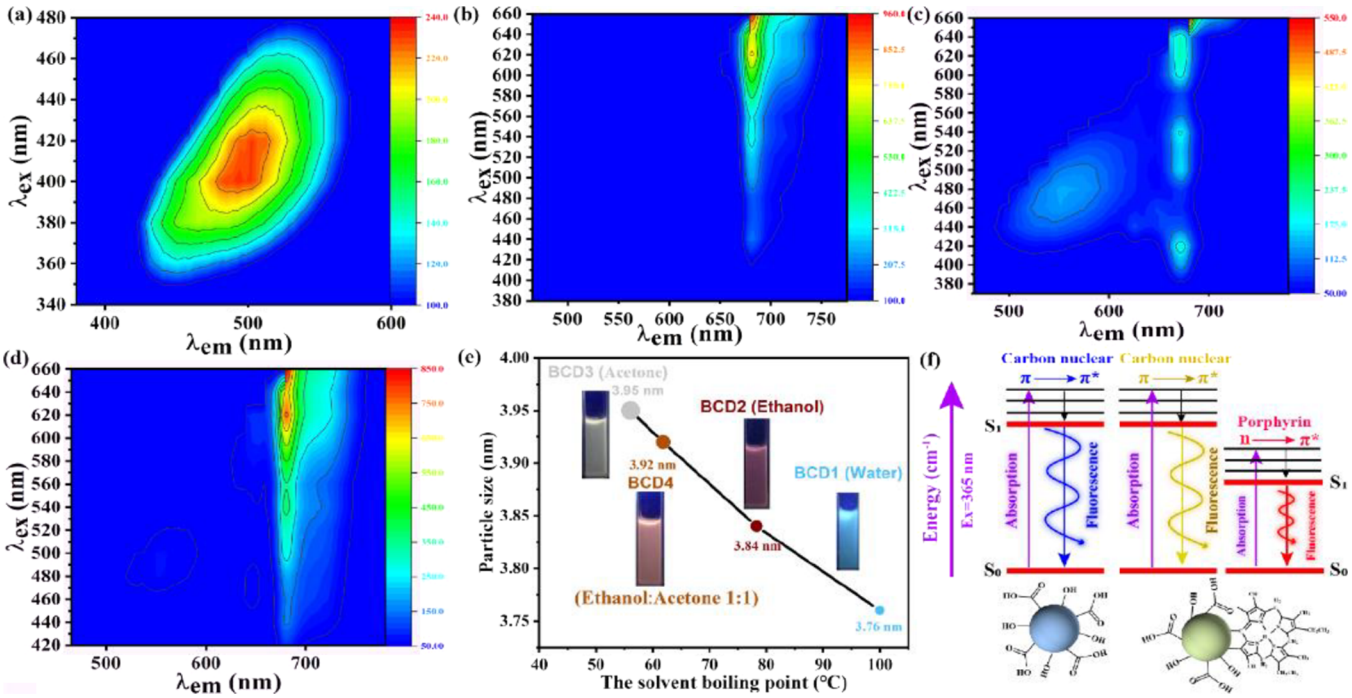

Figure 5. Three-dimensional fluorescence spectra for (a) BCD1, (b) BCD2, (c) BCD3, and (d) BCD4. (e) Influence of boiling point on particle size and optical properties. (f) Band gap transition diagram of blue and red light.

nm; and the solution of BCD1 can emit bright blue light under 365 nm UV light. BCD2, BCD3, and BCD4 present two independent fluorescence emission bands at the blue-to-yellow emission region (400~600 nm) and red emission region (600~750 nm), showing bimodal emission characteristics, with strong emission peaks at 681, 671, and 680 nm, respectively. The solutions of the three samples exhibit different visual colors, which are mainly due to the different intensity ratios of the two bands; BCD2 and BCD4 exhibit crimson and red luminescence under UV light irradiation at 365 nm due to the low-intensity luminescence of the band at the blue-to-yellow emission region. BCD3 shows grayish white fluorescence under UV light irradiation at 365 nm, attributed to an intensity ratio of approximately 1 between the two bands (as shown in Figure S1). In addition, the QYs of BCD2, BCD3, and BCD4 are 12.3, 14.4, and 10.8%, respectively, which indicate relatively high QYs. The photobleaching experiments for all the four types of carbon dots were explored under irradiation with 20 W incandescent lamp for 9 h and 150 W xenon lamp for 60 min, respectively. The experimental results show that the BCDs have good fluorescence stability even if irradiated with 20 W incandescent lamp for 9 h (shown in Figure S2).

3.2. Morphology and Structure of BCDs. The TEM image shows that the four BCDs with quasi-spherical shape exhibit excellent dispersion, and the average particle size is 3.76, 3.84, 3.95, and 3.92 nm, respectively (shown in Figure 2). It can be seen that the luminescence intensity ratio of the two bands is related to the particle size, indicating a size-dependent effect. The high-resolution TEM images of the four BCDs indicate that the as-prepared samples exhibit good lattice fringes with spacings of 0.24, 0.22, 0.23, and 0.24 nm, respectively, which are consistent with the (100) facet of graphitic carbon (shown in the inset of Figure 2). We speculate that the different sizes of the four BCDs are mainly attributed to the different boiling points and polarities of the reaction solvent. As is well known, among the three types of solvents (water, ethanol, and acetone), water has the highest boiling point, while acetone has the lowest boiling point. Under the same preparation conditions, the lower the boiling point, the longer is the carbonization time, which results in the larger particle size of BCDs,[18] being consistent with the results of TEM.

The crystallinity of the four as-obtained BCDs is analyzed by XRD. As shown in Figure 3a, it is found that there are obvious broad diffraction peaks between 19° and 23°, which correspond to the (002) graphite lattice stripes, indicating they are all graphite-like structures.[19] Further, the half-peak width decreases with the decrease of the boiling point of the solvent used for the preparation of BCD1, BCD2, BCD3, and BCD4, which indicates that the degree of graphitization increases accordingly (Table S1). In addition, the Raman spectra of BCD1, BCD2, BCD3, and BCD4 all present two characteristic D (disordered C, sp^3) and G peaks (ordered graphite C, sp^2), which are located at 1330 and 1600 cm^{-1}, respectively.[18] The I_G/I_D values of the four BCDs are 0.63, 0.76, 1.89, and 0.81, respectively (shown in Table S2), indicating that BCD3 contains the largest size of the sp^2-conjugated domain (the degree of graphitization), which is consistent with the results of TEM and XRD. The IR spectra in Figure 3c indicate that the vibration peaks at 3283, 1543, and 1450 cm^{-1} are assigned to the O−H/−NH stretching vibrations of the porphyrin ring, aromatic C=C vibration, and C−N shearing vibration of pyrrole, respectively.[20] The results show that BCD1, BCD2, BCD3, and BCD4 contain the porphyrin structure in chlorophyll.[21] In addition, the bands at 2923, 1659, and 1659 cm^{-1} were attributed to the stretching vibrations of C−H, C=O, and C−O.[21,22]

The elemental composition and surface state of the BCDs were analyzed by XPS (XPS data of spinach powder are shown in Figure S3). As shown in Figure 4a, the full spectra of the four BCDs show that they are mainly composed of C, O, and

https://doi.org/10.1021/acsomega.2c06942
ACS Omega 2023, 8, 6550−6558

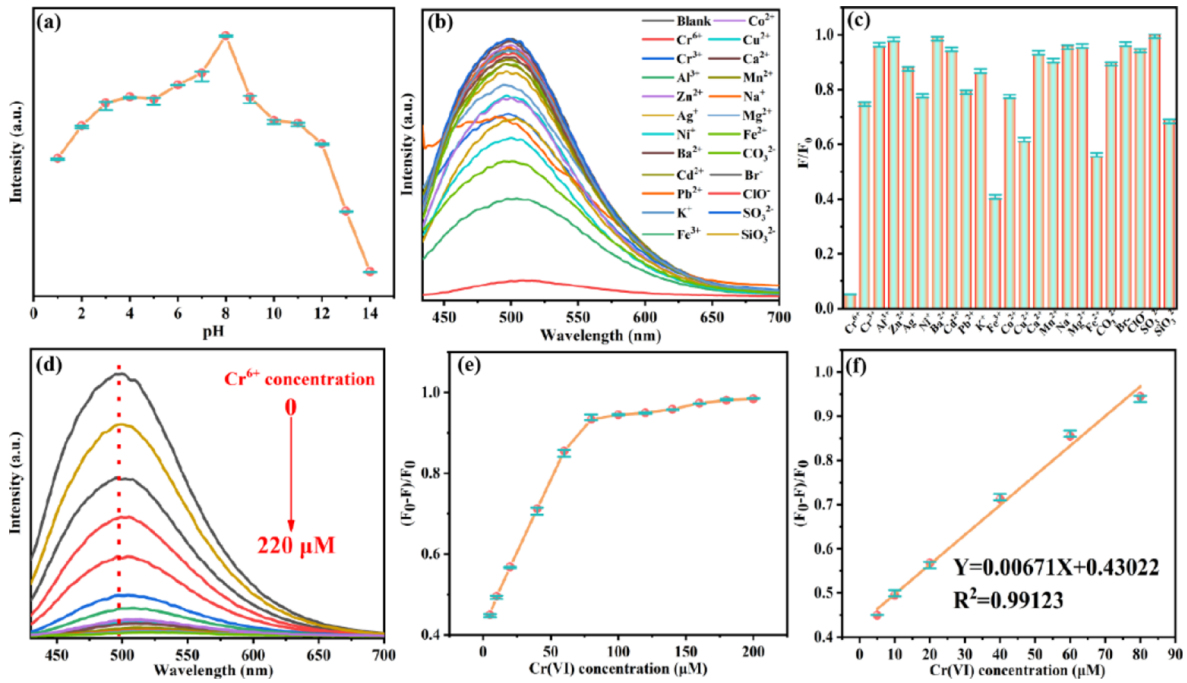

Figure 6. Fluorescence intensity of BCD1 aqueous solution (ex: 400 nm). (a) Different pH values. (b, c) Different ions. (d) Luminescence intensity dependence on the concentration of Cr(VI). (e) Fluorescence intensity ratio (F_0-F/F_0) of BCD1 with various Cr(VI) concentrations in the range of 0−220 μM. (f) Linear relationship of (F_0-F/F_0) with Cr(VI) concentration in the range of 0−80 μM).

N elements with different contents, corresponding to C 1s, O 1s, and N 1s, respectively. The highest content of carbon and the lowest content of oxygen and nitrogen are observed in BCD3, indicating larger conjugated domains and exhibiting a larger particle size,[18] which are mainly ascribed to the lowest boiling point of acetone, being beneficial to the dehydration and carbonization processes of the reaction. The above analysis is consistent with the results of TEM for BCD3 with the largest particle size. The high-resolution XPS spectra of C 1s, O 1s, and N 1s are shown in Figure 4b−d. It is found that there are three peaks at ∼284 eV, corresponding to C−C/C═C, C−O, and C═O, respectively.[23] Interestingly, the intensity of C−C/C═C peaks increases with the decrease of the boiling point, and the C−C/C═C peaks of BCD3 show the highest intensity according to the largest particle size, which further proves the largest size of sp^2 conjugation. Similarly, the boiling point of the reaction solvent also has effects on the O and N contents. The high-resolution XPS spectrum of O 1s has three peaks at ∼530 eV, corresponding to C═O, C−O, and C−OH, respectively.[24] The high-resolution XPS spectrum of N 1s shows three peaks at ∼398 eV, corresponding to C−N−C, N−$(C)_3$, and N−H, consistent with the N element in porphyrin, proving the existence of the porphyrin structure in BCDs.[25] Based on the above analysis results, we can conclude that the different boiling points of the solvent not only affect the size of the synthesized BCDs but also affect their surface states and then their fluorescence properties. In addition, the porphyrin structures on the surface of BCDs play a decisive role in the single excitation and double emission characteristics of BCDs.

3.3. Mechanism of Tunable Fluorescence. In order to elucidate the fluorescence regulation mechanism based on solvent control, the three-dimensional (3D) fluorescence spectra of the four BCDs combined with the influence of boiling point on the particle size and surface state were further explored. Figure 5a presents that BCD1 has a single-emission center corresponding to the blue light wavelength regions, while BCD2, BCD3, and BCD4 have dual-emission centers being associated with the blue-green and red light wavelength regions (Figure 5b−d). Interestingly, different fluorescence intensity ratios of the blue-green and red light wavelength regions (BCD2:3.145, BCD3:0.6, and BCD4:2.812) are found (Figure S1), which realize the tunable luminescence color for BCDs. As is well known, spinach leaves contain polysaccharides and chlorophyll components with a porphyrin structure; we speculate that the blue-green light and red light are ascribed to the carbon core-formed carbonization of the polysaccharide and porphyrin structures on the surface of the carbon core, respectively. The BCD1 aqueous solution presents only blue fluorescence, which is mainly due to the red luminescence quenched in aqueous solution because of the hydrophobic porphyrins. Moreover, the different fluorescence intensity ratios of the blue-green and red light wavelength regions are attributed to the carbonization degree of polysaccharides and chlorophyll. Polysaccharides with the lower boiling point of acetone will undergo a longer carbonization, which results in larger particle size and higher carbon content, indicating the larger conjugation degree and higher luminescence intensity of blue-green light. It is then combined with the red fluorescence emitted by chlorophyll-derived BCDs to emit grayish white fluorescence (Figure 5e). Furthermore, ethanol has a higher boiling point, which results in BCD2 and BCD4 with a lower conjugation degree and low fluorescence intensity, presenting red fluorescence. In addition, the energy-transition mechanism of blue and red light in BCDs is shown in Figure 5f. Under UV excitation, blue light mainly comes from the $\pi-\pi^*$ electron transition of the C═C bond in the carbon nucleus, while red light mainly comes from the $n-\pi^*$ electron transition of the C═O bond in porphyrin derivatives.

https://doi.org/10.1021/acsomega.2c06942
ACS Omega 2023, 8, 6550−6558

4. APPLICATION OF BCDS

4.1. Fluorescence Detection of Hexavalent Chromium Ion (Cr(VI)). In order to further explore the sensing application of BCDs, here, BCD1 was selected as a sensor to detect different ions (Cr^{6+}, Cr^{3+}, Al^{3+}, Zn^{2+}, Ag^{+}, Ni^{+}, Ba^{2+}, Cd^{2+}, Pb^{2+}, K^{+}, Fe^{3+}, Co^{2+}, Cu^{2+}, Ca^{2+}, Mn^{2+}, Na^{+}, Mg^{2+}, Fe^{2+}, CO_3^{2-}, Br^{-}, ClO^{-}, SO_3^{2-}, and SiO_3^{2-}) with a concentration of 10 mM, and the excitation wavelength was fixed at 400 nm. First, the influence of pH value on the fluorescence intensity of BCD1 was tested. It can be seen from Figure 6a that the fluorescence intensity has a maximum value when pH = 8, so the following ion detection experiment was carried out in buffer solution with pH = 8. Figure 6b,c indicates that Cr(VI) has a significant fluorescence quenching effect compared with other metal ions, and about 95% quenching rate is observed in the Cr(VI) solution, indicating that BCD1 shows a high sensitive selective detection of Cr(VI) ions.

Consequently, the fluorescence intensity of BCD1 with different concentrations of Cr(VI) was studied. As shown in Figure 6d, it is found that the fluorescence intensity of BCD1 decreased gradually with the increase of Cr(VI) concentration (0∼220 μM) in aqueous solution. Figure 6e presents the relationship between the F_0-F/F_0 value and Cr(VI) concentration, where F_0 and F represent the fluorescence intensities in the absence and presence of Cr(VI). The linear equation is $F_0-F/F_0 = 0.00671x + 0.99123$ in the 0−220 μM concentration range, where x represents the Cr(VI) concentration, and the correlation coefficient (R^2) is 0.99123. According to the equation LOD = 3σ/S, LOD was 0.242 μM, where σ is the generalized triple standard deviation of fluorescence intensity of 11 blank samples of the BCD1 solution, and S is the slope of the linear relationship between F_0-F/F_0 and Cr(VI) concentration. The results showed that spinach-based BCD1 was highly sensitive to Cr(VI) with a LOD of 0.242 μM. The World Health Organization (WHO) proposed a provisional guideline of total chromium intake of human body of 0.05 mg/L (0.96 μM), indicating that the sensitivity of BCD1 to Cr(VI) fully meets the requirements of WHO for the detection of Cr(VI) in liquid samples.[26] Compared with other methods, the sensing detection of Cr(VI) based on BCD1 fluorescence quenching shows a higher selective sensitivity and a wider detection range (shown in Table S3). Furthermore, the intraday and interday experiments reveal that the fluorescence response of BCD1 to Cr(VI) has excellent stability and reproducibility. Further, the recovery rate of Cr(VI) spike based on BCD1 was 101.73−105.22%, and RSD < 2.99% (shown in Table 1).

4.2. Quantitative Detection of Cr(VI) in Environmental Water Samples. Tap water and river water were selected to unveil the practical application of Cr(VI) detection in environmental water samples. The above water samples were spiked with different concentrations of Cr(VI) ions (20, 40, and 60 μM), and an overview of the respective retrievals could be found in Table 2. The fluorescence responses of BCD1 to Cr(VI) concentrations were 20.41, 41.58, and 60.91 μM in tap water and 20.96, 41.81, and 64.51 μM in river water, respectively. Simultaneously, the spiked recoveries of Cr(VI) based on BCD1 were calculated to be 101.52−107.51%, with RSD < 1.15%, which indicated that the BCD1-based sensing platform was highly accurate and practical for the detection of Cr(VI) ions in environmental water samples.

Table 1. Detection of Cr(VI) in Different Water Samples (n = 5)

sample	spiked (μM)	found (μM)	recovery (%)	RSD (%)
intraday (n = 5)	20	20.35	101.73	0.69
	40	41.74	104.35	0.41
	60	61.06	101.78	0.17
interday (n = 5)	20	20.56	102.81	1.73
	40	41.75	104.38	0.24
	60	63.13	105.22	2.99

Table 2. Detection of Cr(VI) in Different Water Samples (n = 5)

sample	spiked (μM)	found (μM)	recovery (%)	RSD (%)
tap water	20	20.41	102.05	0.92
	40	41.58	104.63	0.6
	60	60.91	101.52	1.15
river water	20	20.96	104.81	0.94
	40	41.81	104.53	0.36
	60	64.51	107.51	0.12

4.3. Fluorescence Anti-Counterfeiting. Multicolor BCDs, used as fluorescent inks, have potential application prospects in anti-counterfeiting due to their adjustable fluorescence properties, strong stability, low cost, and ecofriendly synthesis method.[27] Figure 7a shows the lotus anti-counterfeiting pattern drawn on a filter paper using BCDs as fluorescent inks under sunlight. Incredibly, a vivid picture of a multicolor lotus emerges under 365 nm excitation, showing advanced fluorescence anti-counterfeiting effects. Consequently, delicate anti-counterfeiting patterns were obtained using the as-synthesized multicolor BCDs as fluorescent inks by inkjet printing technology. As shown in Figure 7b, the printed patterns of Chinese panda are almost invisible under sunlight, but the colorful logo with bright blue, white, and red fluorescence appear under a UV lamp (365 nm). Further, the colorful patterns disappear completely when the 365 nm UV lamp is turned off, which can result in achieving high-quality information encryption and decryption effects. Moreover, the inkjet-printed colorful patterns can maintain high fluorescence

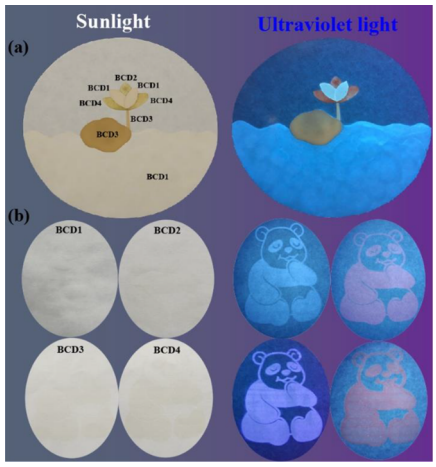

Figure 7. Anti-counterfeiting patterns of (a) lotus and (b) Chinese panda obtained using multicolor BCDs as fluorescent inks by hand drawing and inkjet printing, respectively (left: under sunlight; right: under UV light).

https://doi.org/10.1021/acsomega.2c06942
ACS Omega 2023, 8, 6550−6558

stability for several months, indicating that the ecofriendly fluorescent ink based on the as-gained BCDs has better durability and reliability.

5. CONCLUSIONS

In summary, multicolor BCDs with single excitation and multiple emission characteristics were prepared by a facile and ecofriendly solvothermal method using spinach as the carbon source based on solvent control. The four as-obtained adjustable BCDs can emit blue, crimson, grayish white, and red luminescence, which almost cover the range of the UV−infrared emission. The QY values of the four BCDs were up to 8.9, 12.3, 14.4, and 10.8%, respectively. Further studies proved that the conjugation degree of carbon nucleus and the luminescence characteristics of porphyrin are the main reasons for the change in the fluorescence properties of BCDs. Interestingly, BCD1 shows excellent selective and sensitive detection of Cr(VI), with the detection limit of 0.242 μM, and the intraday and interday relative standard deviations are less than 2.99%. More importantly, the recovery of tap water and river by the investigated Cr(VI) sensor was found to be 101.52 to 107.51%, which indicates that the Cr(VI) sensor based on BCD1 has superior advantages of sensitivity, selectivity, rapidity, and reproducibility. Furthermore, the four BCDs obtained can be used as fluorescent inks to print the patterns of lotus and Chinese panda, presenting high-precision visual information encryption. This study presents a novel simple ecofriendly synthesis method of high-quality multicolor luminous BCDs from natural resources, which have good application prospects in ion detection and advanced anti-counterfeiting.

■ ASSOCIATED CONTENT

Supporting Information

The Supporting Information is available free of charge at https://pubs.acs.org/doi/10.1021/acsomega.2c06942.

Normalized fluorescence spectra of BCDs; fluorescence intensity ratio of red and blue-yellow regions for BCDs; photostability experiment of BCDs; XPS analysis of spinach powder; peak position and FWHM of BCDs; relationship between ID and IG of four BCDs; and comparation of different BCDs for the sensing of Cr(VI) (PDF)

■ AUTHOR INFORMATION

Corresponding Authors

Qian Cheng − *Key Laboratory of Bio-Based Material Science & Technology (Ministry of Education), College of Material Science and Engineering, Northeast Forestry University, Harbin 150040, P. R. China;* orcid.org/0000-0002-4776-3887; Email: chengqian66@163.com

Yu Li − *College of Science, Northeast Forestry University, Harbin 150040, P. R. China*; Email: liyu87043@163.com

Shouxin Liu − *Key Laboratory of Bio-Based Material Science & Technology (Ministry of Education), College of Material Science and Engineering, Northeast Forestry University, Harbin 150040, P. R. China;* orcid.org/0000-0002-0491-8885; Email: liushouxin@126.com

Authors

Shipeng Wang − *Key Laboratory of Bio-Based Material Science & Technology (Ministry of Education), College of Material Science and Engineering, Northeast Forestry University, Harbin 150040, P. R. China;* orcid.org/0000-0001-9589-0007

Haoran Zhao − *Key Laboratory of Bio-Based Material Science & Technology (Ministry of Education), College of Material Science and Engineering, Northeast Forestry University, Harbin 150040, P. R. China*

Jinliang Yang − *Key Laboratory of Bio-Based Material Science & Technology (Ministry of Education), College of Material Science and Engineering, Northeast Forestry University, Harbin 150040, P. R. China*

Yahui Dong − *Key Laboratory of Bio-Based Material Science & Technology (Ministry of Education), College of Material Science and Engineering, Northeast Forestry University, Harbin 150040, P. R. China*

Shaozheng Guo − *College of Chemistry and Chemical Engineering, Shaoxing University, Shaoxing, Zhejiang 312000, China*

Complete contact information is available at: https://pubs.acs.org/10.1021/acsomega.2c06942

Notes

The authors declare no competing financial interest.

■ ACKNOWLEDGMENTS

This work was supported by the Fundamental Research Funds for the Central Universities (2572019BB06), Heilongjiang Provincial Natural Science Foundation of China (LH2019E002), and National Natural Science Foundation of China (31890773).

■ ABBREVIATIONS

CDs	carbon dots
BCDs	biomass carbon dots
QY	quantum yield
LOD	limit of detection
WHO	World Health Organization

■ REFERENCES

(1) Yang, H.; Liu, Y.; Guo, Z.; Lei, B.; Zhuang, J.; Zhang, X.; Liu, Z.; Hu, C. Hydrophobic Carbon Dots with Blue Dispersed Emission and Red Aggregation-Induced Emission. *Nat. Commun.* **2019**, *10*, 1789.

(2) Huo, F.; Karmaker, P. G.; Liu, Y.; Zhao, B.; Yang, X. Preparation and Biomedical Applications of Multicolor Carbon Dots: Recent Advances and Future Challenges. *Part. Part. Syst. Charact.* **2020**, *37*, No. 1900489.

(3) Zhu, L.; Shen, D.; Liu, Q.; Wu, C.; Gu, S. Sustainable Synthesis of Bright Green Fluorescent Carbon Quantum Dots from Lignin for Highly Sensitive Detection of Fe3+ Ions. *Appl. Surf. Sci.* **2021**, *565*, No. 150526.

(4) Li, Y.; Bai, G.; Zeng, S.; Hao, J. Theranostic Carbon Dots with Innovative NIR-II Emission for in Vivo Renal-Excreted Optical Imaging and Photothermal Therapy. *ACS Appl. Mater. Interfaces* **2019**, *11*, 4737−4744.

(5) Bayda, S.; Hadla, M.; Palazzolo, S.; Kumar, V.; Caligiuri, I.; Ambrosi, E.; Pontoglio, E.; Agostini, M.; Tuccinardi, T.; Benedetti, A.; Riello, P.; Canzonieri, V.; Corona, G.; Toffoli, G.; Rizzolio, F. Bottom-up Synthesis of Carbon Nanoparticles with Higher Doxorubicin Efficacy. *J. Controlled Release* **2017**, *248*, 144−152.

(6) Achilleos, D. S.; Kasap, H.; Reisner, E. Photocatalytic Hydrogen Generation Coupled to Pollutant Utilisation Using Carbon Dots Produced from Biomass. *Green Chem.* **2020**, *22*, 2831−2839.

(7) Park, S. J.; Park, J. Y.; Chung, J. W.; Yang, H. K.; Moon, B. K.; Yi, S. S. Color Tunable Carbon Quantum Dots from Wasted Paper by

Different Solvents for Anti-Counterfeiting and Fluorescent Flexible Film. *Chem. Eng. J.* **2020**, *383*, No. 123200.
(8) Zhu, S.; Meng, Q.; Wang, L.; Zhang, J.; Song, Y.; Jin, H.; Zhang, K.; Sun, H.; Wang, H.; Yang, B. Highly Photoluminescent Carbon Dots for Multicolor Patterning, Sensors, and Bioimaging. *Angew. Chem., Int. Ed.* **2013**, *52*, 3953−3957.
(9) Yan, F.; Jiang, Y.; Sun, X.; Bai, Z.; Zhang, Y.; Zhou, X. Surface Modification and Chemical Functionalization of Carbon Dots: A Review. *Microchim. Acta* **2018**, *185*, 424.
(10) Wijesekera, T. P.; Dolphin, D. *Some Preparations and Properties of Porphyrins BT-Methods in Porphyrin Photosensitization*; Kessel, D., Ed.; Springer US: Boston, MA, 1985; pp 229−266.
(11) Liu, R.; Zhang, L.; Zhao, J.; Hou, C.; Huang, Y.; Huang, Z.; Zhao, S. A Distinctive Spinach-Based Carbon Nanomaterial with Chlorophyll-Rich and Near-Infrared Emission for Simultaneous In Vivo Biothiol Imaging and Dual-Enhanced Photodynamic Therapy of Tumor. *Adv. Ther.* **2019**, *2*, No. 1900011.
(12) Wang, P.; Yan, Y.; Zhang, Y.; Gao, T.; Ji, H.; Guo, S.; Wang, K.; Xing, J.; Dong, Y. An Improved Synthesis of Water-Soluble Dual Fluorescence Emission Carbon Dots from Holly Leaves for Accurate Detection of Mercury Ions in Living Cells. *Int. J. Nanomed.* **2021**, *16*, 2045−2058.
(13) Cui, Y.; Liu, R.; Ye, F.; Zhao, S. Single-Excitation, Dual-Emission Biomass Quantum Dots: Preparation and Application for Ratiometric Fluorescence Imaging of Coenzyme A in Living Cells. *Nanoscale* **2019**, *11*, 9270−9275.
(14) Liu, J.; Kong, T.; Xiong, H.-M. Mulberry-Leaves-Derived Red-Emissive Carbon Dots for Feeding Silkworms to Produce Brightly Fluorescent Silk. *Adv. Mater.* **2022**, *34*, No. 2200152.
(15) Yan, F.; Jiang, Y.; Sun, X.; Wei, J.; Chen, L.; Zhang, Y. Multicolor Carbon Dots with Concentration-Tunable Fluorescence and Solvent-Affected Aggregation States for White Light-Emitting Diodes. *Nano Res.* **2020**, *13*, 52−60.
(16) Long, P.; Feng, Y.; Cao, C.; Li, Y.; Han, J.; Li, S.; Peng, C.; Li, Z.; Feng, W. Self-Protective Room-Temperature Phosphorescence of Fluorine and Nitrogen Codoped Carbon Dots. *Adv. Funct. Mater.* **2018**, *28*, No. 1800791.
(17) Li, L.; Zhang, R.; Lu, C.; Sun, J.; Wang, L.; Qu, B.; Li, T.; Liu, Y.; Li, S. In Situ Synthesis of NIR-Light Emitting Carbon Dots Derived from Spinach for Bio-Imaging Applications. *J. Mater. Chem. B* **2017**, *5*, 7328−7334.
(18) Sun, Z.; Yan, F.; Xu, J.; Zhang, H.; Chen, L. Solvent-Controlled Synthesis Strategy of Multicolor Emission Carbon Dots and Its Applications in Sensing and Light-Emitting Devices. *Nano Res.* **2022**, *15*, 414−422.
(19) Amjadi, M.; Shokri, R.; Hallaj, T. A New Turn-off Fluorescence Probe Based on Graphene Quantum Dots for Detection of Au (III) Ion. *Spectrochim. Acta, Part A* **2016**, *153*, 619−624.
(20) Ardekani, S. M.; Dehghani, A.; Hassan, M.; Kianinia, M.; Aharonovich, I.; Gomes, V. G. Two-Photon Excitation Triggers Combined Chemo-Photothermal Therapy via Doped Carbon Nano-hybrid Dots for Effective Breast Cancer Treatment. *Chem. Eng. J.* **2017**, *330*, 651−662.
(21) Frasco, M. F.; Vamvakaki, V.; Chaniotakis, N. Porphyrin Decorated CdSe Quantum Dots for Direct Fluorescent Sensing of Metal Ions. *J. Nanopart. Res.* **2010**, *12*, 1449−1458.
(22) Sangam, S.; Gupta, A.; Shakeel, A.; Bhattacharya, R.; Sharma, A. K.; Suhag, D.; Chakrabarti, S.; Garg, S. K.; Chattopadhyay, S.; Basu, B.; Kumar, V.; Rajput, S. K.; Dutta, M. K.; Mukherjee, M. Sustainable Synthesis of Single Crystalline Sulphur-Doped Graphene Quantum Dots for Bioimaging and Beyond. *Green Chem.* **2018**, *20*, 4245−4259.
(23) Goswami, J.; Rohman, S. S.; Guha, A. K.; Basyach, P.; Sonowal, K.; Borah, S. P.; Saikia, L.; Hazarika, P. Phosphoric Acid Assisted Synthesis of Fluorescent Carbon Dots from Waste Biomass for Detection of Cr(VI) in Aqueous Media. *Mater. Chem. Phys.* **2022**, *286*, No. 126133.
(24) Qu, K.; Chen, M.; Wang, W.; Yang, S.; Jing, S.; Guo, S.; Tian, J.; Qi, H.; Huang, Z. Biomass-Derived Carbon Dots Regulating Nickel Cobalt Layered Double Hydroxide from 2D Nanosheets to 3D Flower-like Spheres as Electrodes for Enhanced Asymmetric Supercapacitors. *J. Colloid Interface Sci.* **2022**, *616*, 584−594.
(25) Yu, X.; Huo, Y.; Yang, J.; Chang, S.; Ma, Y.; Huang, W. Reduced Graphene Oxide Supported Au Nanoparticles as an Efficient Catalyst for Aerobic Oxidation of Benzyl Alcohol. *Appl. Surf. Sci.* **2013**, *280*, 450−455.
(26) Hu, G.; Ge, L.; Li, Y.; Mukhtar, M.; Shen, B.; Yang, D.; Li, J. Carbon Dots Derived from Flax Straw for Highly Sensitive and Selective Detections of Cobalt, Chromium, and Ascorbic Acid. *J. Colloid Interface Sci.* **2020**, *579*, 96−108.
(27) Guo, J.; Li, H.; Ling, L.; Li, G.; Cheng, R.; Lu, X.; Xie, A.-Q.; Li, Q.; Wang, C.-F.; Chen, S. Green Synthesis of Carbon Dots toward Anti-Counterfeiting. *ACS Sustainable Chem. Eng.* **2020**, *8*, 1566−1572.

https://doi.org/10.1021/acsomega.2c06942
ACS Omega 2023, 8, 6550−6558